AUTHOR QUERY FORM

Dear Author,

Please check your proof carefully and mark all corrections at the appropriate place in the proof (e.g., by using on-screen annotation in the PDF file) or compile them in a separate list. Note: if you opt to annotate the file with software other than Adobe Reader then please also highlight the appropriate place in the PDF file. To ensure fast publication of your paper please return your corrections within 48 hours.

For correction or revision of any artwork, please consult http://www.elsevier.com/artworkinstructions.

Any queries or remarks that have arisen during the processing of your manuscript are listed below and highlighted by flags in the proof. Click on the 'Q' link to go to the location in the proof.

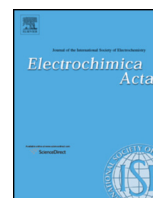| Location in article	Query / Remark: **click on the Q link to go** **Please insert your reply or correction at the corresponding line in the proof**
Q1	Please confirm that given names and surnames have been identified correctly. Please check this box or indicate your approval if you have no corrections to make to the PDF file ☐

 Thank you for your assistance.

The specific capacitance of sol–gel synthesised spinel MnCo$_2$O$_4$ in an alkaline electrolyte

Q1 Ling-Bin Kong[a,b,*], Chao Lu[a], Mao-Cheng Liu[a], Yong-Chun Luo[b], Long Kang[b], Xiaohong Li[c], Frank C. Walsh[c]

[a] State Key Laboratory of Gansu Advanced Non-Ferrous Metal Materials, Lanzhou University of Technology, Lanzhou 730050, PR China
[b] School of Materials Science and Engineering, Lanzhou University of Technology, Lanzhou 730050, PR China
[c] Electrochemical Engineering Laboratory, Energy Technology Research Group, Faculty of Engineering and the Environment, University of Southampton, Highfield, Southampton SO17 1BJ, United Kingdom

ARTICLE INFO

ABSTRACT

In this work, high performance spinel MnCo$_2$O$_4$ electrode was fabricated via a facile sol–gel method and its capacitive behavior was successfully investigated in alkaline electrolyte. MnCo$_2$O$_4$ electrode was characterized by means of powder X-ray diffraction (XRD), scanning electron microscopy (SEM), and transmission electron microscope (TEM). The pseudo capacitive behavior of spinel MnCo$_2$O$_4$ was widely investigated in 2 M KOH aqueous electrolyte using cyclic voltammetry (CV), galvanostatic charge-discharge test, and electrochemical impedance spectroscopy (EIS). As a result, the spinel MnCo$_2$O$_4$ exhibited excellent porous structure and the highest specific capacitance of 405 F g^{-1} was achieved at a current density of 5 mA cm^{-2}. In addition, the spinel MnCo$_2$O$_4$ displayed desirable stability in alkaline electrolyte during long-term cycles with a cycling efficiency of 95.1% over 1,000 cycles. The high specific capacitance and excellent cycling ability of MnCo$_2$O$_4$ show promise for its application in supercapacitors.

© 2013 Published by Elsevier Ltd.

1. Introduction

High-performance electrical energy storage technologies are urgently needed in today's mobile, information-rich and energy-conscious society. Herein, electrochemical supercapacitors are receiving considerable attention as charge-storage devices [1]. Generally, faradic pseudo capacitors based on metal oxides (Ni, Co, Mn, etc.) have a higher energy density and specific capacitance than those of most commercial supercapacitors made of carbon materials [2,3]. Among metal oxides, Co oxides are normally reported to have high redox activity and good reversibility, but specific capacitance is relatively low [4]. Some Co-based oxides or Co hydroxides have been reported to exhibit high specific capacitance [5–7]. However, carbon nanotube or nanofiber seems to be one important reason in improving their specific capacitance. In order to further raise specific capacitance of Co oxides, we prepared NiCo$_2$O$_4$ in our previous work [8], but it displayed obvious polarization and undesirable charge-discharge platform. Thus, the development of alternative electrode materials is next logical step.

In our work, a spinel MnCo$_2$O$_4$ was successfully prepared by using a facile sol–gel method. Generally, Mn oxides have relatively low specific capacitance and partial dissolution in alkaline electrolyte also leads to decay in capacitance [9–11]. Besides, Mn oxides have a poor electronic [12] and ionic conductivity [13,14]. Recently, researchers find that binary metal oxides are quite intriguing from the perspectives of both fundamental science and technology because the composite can enable versatile and tailor-made properties with performances far beyond those of monometallic oxides [15]. For example, according to relevant literature [16], binary metal oxides may possess a higher electronic conductivity and higher electrochemical activity than those of monometallic oxides. The addition of other transition metal oxides also has proven to be an effective way to improve the electrochemical properties. Therefore, Mn-Co binary metal oxides have caught our attention since they seem to possess multiple oxidation states/structures, enabling rich redox reactions for faradic pseudo capacitance generation. Wei's group [17–19] demonstrated the nanocrystalline coatings, defective rock-salt structure, and rock salt-spinel structural transformation of Mn-Co oxides, but they paid no attention to their electrochemical performances. Prasad and Miura [20] reported that the addition of Co oxide can boost specific capacitance of Mn oxide electrodes. Chang's group [21] prepared Mn-Co oxides by anodic deposition, founding that the addition of an appropriate amount of Co can enhance the electrochemical reversibility and

* Corresponding author at: Lanzhou University of Technology, State Key Laboratory of Gansu Advanced Non-ferrous Metal Materials, 287 Langongping Road, Lanzhou, China. Tel.: +86 931 2976579; fax: +86 931 2976578.
E-mail address: konglb@lut.cn (L.-B. Kong).

stability. The Mn-Co oxides exhibited a highest specific capacitance of 186 F g^{-1} in neutral electrolyte and 75% of the initial specific capacitance remained after 500 cycles. Yang [22] reported that the 3.0% Co-doped Mn$_{0.970}$Co$_{0.030}$O$_x$ film exhibited the highest specific capacitance of 99 F g^{-1} at a 5 mV s^{-1} scan rate in neutral electrolyte. Chuang and Hu [23] reported that Co-doped Mn oxide has the specific capacitance of 125 F g^{-1} (measured at 25 mV s^{-1} in neutral electrolyte). Li's group [10] prepared Mn-Co oxides (CMOs) by chemical method. The specific capacitance of CMOs reached 360 F g^{-1} when CMOs were heated at 800 °C. But it displayed unfavorable stability within the only 20 charge-discharge cycles due to the partial dissolution in alkaline electrolyte. Babakhani's group [24] prepared Mn-Co oxides by anodic deposition with the specific capacitance of 213 F g^{-1} in neutral electrolyte. After 500 cycles, the fading of specific capacitance was about 18%.

Thus, from the existing literatures about Mn-Co oxides, some drawbacks can be summarized as follows: (1) Electrodeposition methods reported so far are not practical for commercial production because they are either slow in the growth of very thin layer on thick substrates or expensive for large scale industrial production. (2) Mn-Co oxides have relatively low specific capacitance in neutral electrolyte. They displayed much higher specific capacitance in alkaline electrolyte, but the partial dissolution was adverse factor. In contrast, our sol–gel method is more suitable for large scale commercial production because of facility, low-cost, and high yield. Compared with the dissolution of reported Mn-Co oxides in alkaline electrolyte, the successful application of alkaline electrolyte has greatly increased the capacity of MnCo$_2$O$_4$. So far, sol–gel method has never been used to prepare MnCo$_2$O$_4$ and our preliminary exploitation, using a sol–gel technique, raises the expectation of a facile synthesis of high performance MnCo$_2$O$_4$. Moreover, there was no apparent polarization and charge-discharge platform.

2. Experimental

2.1. Preparation of the MnCo$_2$O$_4$ materials

All of the chemicals were of analytical grade and used without further purification. MnCl$_2$·4H$_2$O and CoCl$_2$·6H$_2$O were all purchased from Sinopharm Chemical Reagent Co. Ltd. Nickel foam was purchased from ChangSha Lyrun New Material Co. Ltd. The nickel foam was washed in acetone with ultrasonic for 30 min at first, then washed with double-distilled water for several times and dried in an oven at 60 °C. 0.154 g MnCl$_2$·4H$_2$O and 0.37 g CoCl$_2$·6H$_2$O were dissolved in 1.975 g ethanol in a glass beaker. Then 1.495 g propylene oxide was added and the mixture was stirred at room temperature for another 12 h. The resulting solution was then stirred at 75 °C to promote gelation. The purple gel was heated in air at 200, 250, 300 or 350 °C for 5 h. The resulting samples were washed with ethanol and distilled water for several times, and then dried at 80 °C for 12 h. In addition, for comparative purpose, Co$_3$O$_4$ and Mn$_3$O$_4$ were prepared via the same method when MnCl$_2$·4H$_2$O and CoCl$_2$·6H$_2$O are employed as reactant respectively. The next procedures are the same as that for preparing MnCo$_2$O$_4$.

2.2. Structure characterization

Crystallite structures were determined by X-ray diffraction (XRD) using a Rigaku D/MAX 2400 diffractometer (Japan) with Cu Kα radiation (λ = 1.5418 Å) operating at 40 kV and 60 mA. The microstructure was characterized by transmission electron microscopy (TEM, JEOL, JEM-2010, Japan) operating at 200 kV and 10 μA. The morphology was characterized by field emission scanning electron microscopy (SEM, JEOL, JSM-6701F, Japan) with an accelerated voltage of 5 kV. In addition, the pore properties,

including the BET surface area and pore size distribution were investigated volumetrically by nitrogen adsorption/desorption experiments (ASAP 2020).

2.3. Preparation of the electrode

The working electrodes were prepared according to our previous work [8]. 80 wt.% of electroactive material was mixed with 7.5 wt.% of acetylene black and 7.5 wt.% of conducting graphite in an agate mortar until a homogeneous black powder was obtained. To this mixture, 5 wt.% of poly (tetrafluoroethylene) was added together with a few drops of ethanol. The resulting paste was pressed at 10 MPa into a nickel foam (ChangSha Lyrun New Material Co. Ltd., 90 PPI, 2 mm) then dried at 80 °C for 12 h.

2.4. Electrochemical test of the single electrode

The mass of electroactive material (MnCo$_2$O$_4$, Co$_3$O$_4$, or Mn$_3$O$_4$) was 8 mg. A typical three-electrode glass cell equipped with a working electrode, a platinum foil counter electrode, and a saturated calomel reference electrode (SCE) was used for electrochemical measurements of the as-prepared working electrodes. All electrochemical measurements were carried out using a working electrode area of 1 cm^2 in 2 M KOH electrolyte using an electrochemical working station (CHI660C, Shanghai, China) at 25 °C. Cyclic voltammetry (CV), galvanostatic charge-discharge, electrochemical impedance spectroscopy (EIS), and cycling stability test were carried out.

3. Results and discussion

3.1. Structure and surface morphology characterization

The crystal phase and structure information were obtained by XRD measurements. Fig. 1a shows the XRD patterns of products calcined at 200, 250, 300, and 350 °C for 5 h, respectively. The sample prepared at 200 or 250 °C is accompanied by some Co(OH)$_2$ and Mn$_3$O$_4$. It can be seen that MnCo$_2$O$_4$ prepared at 300 or 350 °C is well-crystallized, which can be discerned from the diffraction peaks. The peaks at 2θ of 18.55, 30.54, 36.00, 37.64, 43.76, 54.34, 57.91, and 63.62° can be indexed as (1 1 1), (2 2 0), (3 1 1), (2 2 2), (4 0 0), (4 2 2), (5 1 1), and (4 4 0) crystal plane. The resultant diffraction peaks corroborate well with the standard pattern of spinel MnCo$_2$O$_4$ (PDF, card no 23-1237, cubic crystal system) and no peaks of other phases are detectable. In addition, the crystal lattice parameter (a = b = c = 8.2720 Å) calculated from the XRD results of sample prepared at 300 °C is highly similar with the standard data (a = b = c = 8.2690 Å) of MnCo$_2$O$_4$. It also can be calculated that the average grain size of MnCo$_2$O$_4$ by applying Scherrer's equation (Dc = 0.89 λ/(β cosθ)). With further increase in the calcinations temperature from 300 to 350 °C, MnCo$_2$O$_4$ experienced a grain-size increase from 8.2 nm to 13.6 nm estimated from the (3 1 1). In addition, Mn$_3$O$_4$ and Co$_3$O$_4$ were successfully prepared via the same method. Fig. 1b shows the X-ray diffraction patterns of Mn$_3$O$_4$ and Co$_3$O$_4$ prepared at 300 °C. The resultant diffraction peaks corroborate well with the standard pattern of Mn$_3$O$_4$ (PDF, card no 24-0734) and Co$_3$O$_4$ (PDF, card no 42-1467).
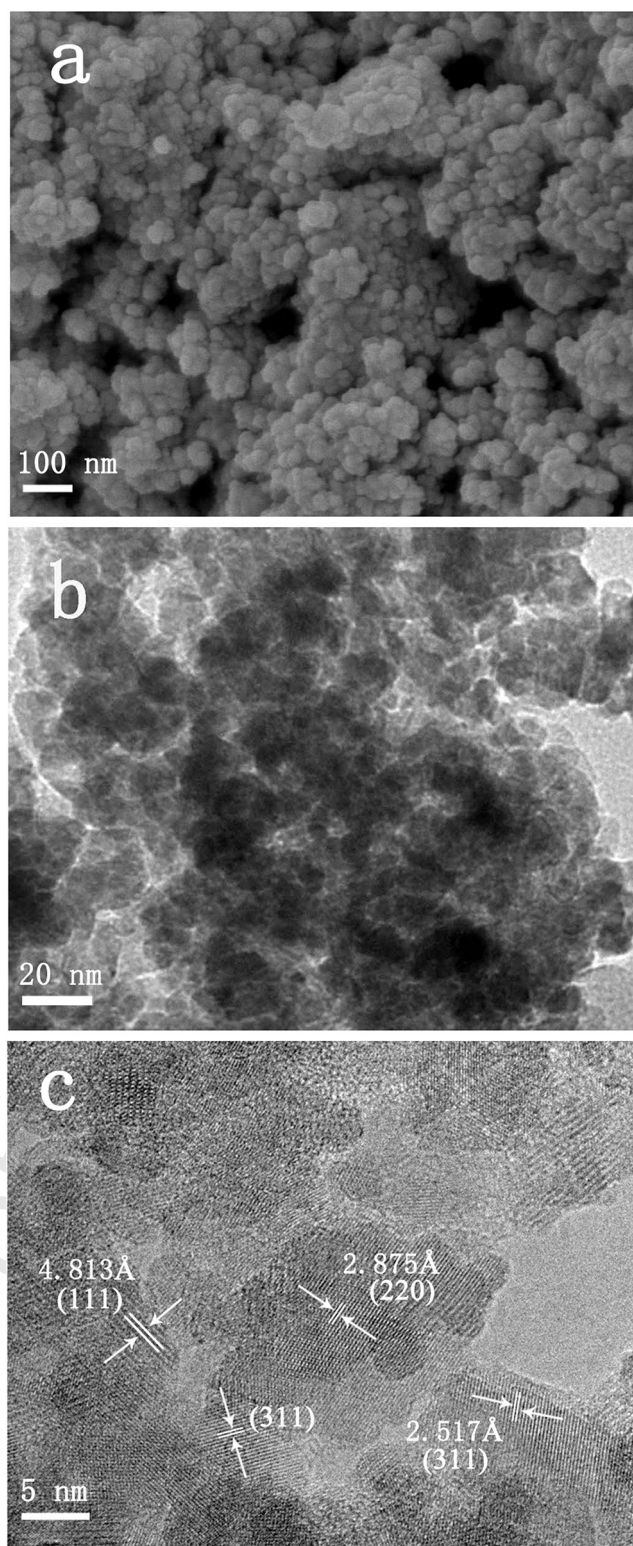
Detailed structural information was further obtained using SEM and TEM. The surface morphology and microstructure of product calcined at 300 °C are presented in Fig. 2a–c. A loosely packed porous structure consisting of interconnected nanoparticles was clearly displayed in Fig. 3a. Numerous macropores and mesopores are evident, which are in favor of improving the power performance. It is well documented that macropores can serve as ion buffering reservoirs and mesopores are capable of overcoming the
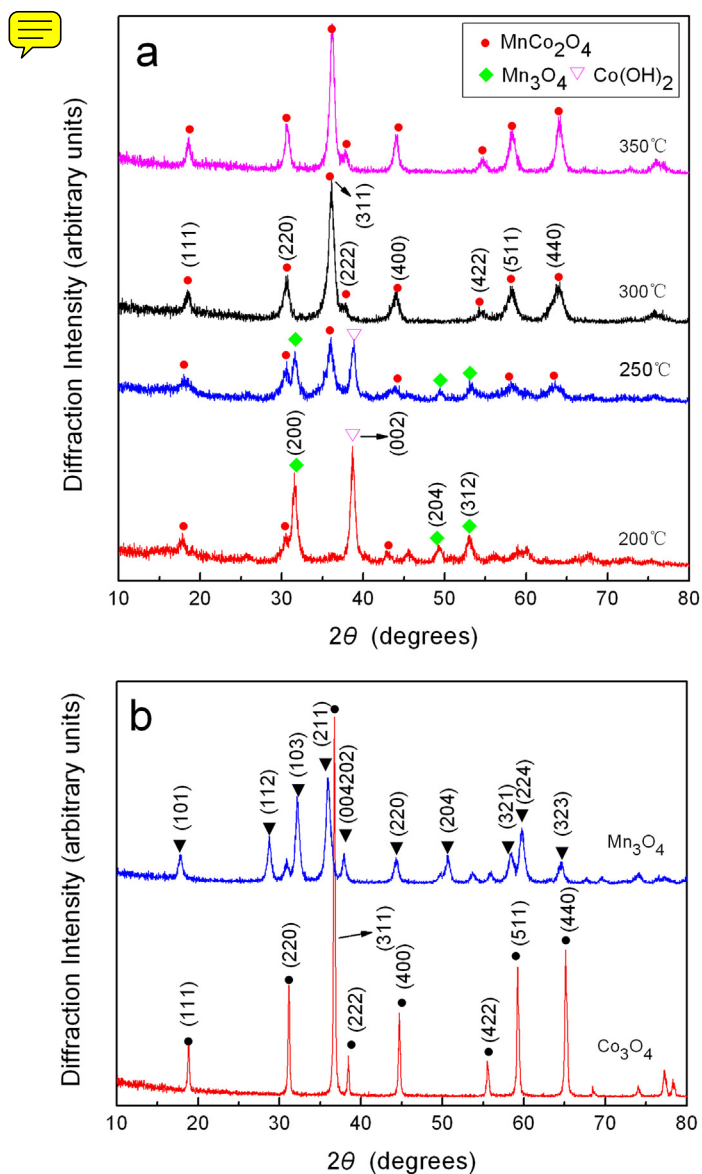
Fig. 1. (a) The X-ray diffraction patterns of products calcined at 200, 250, 300 and 350 °C, respectively; (b) The X-ray diffraction patterns of Mn_3O_4 and Co_3O_4 prepared at 300 °C.

Fig. 2. (a) The SEM image of $MnCo_2O_4$; (b) The TEM image of $MnCo_2O_4$; (c) The HRTEM image of $MnCo_2O_4$.

primary kinetic limits of electrochemical processes [25]. Furthermore, Fig. 2b exhibits granular structure with some chink. This is in accordance with the results of SEM imaging shown in Fig. 2a. The high-resolution TEM investigation (Fig. 2c) demonstrates that the interplanar distances of 4.813, 2.875, and 2.517 Å are highly consistent with the standard interplanar distances of 4.780, 2.925, and 2.493 Å which correspond with (1 1 1), (2 2 0), and (3 1 1) crystal planes. Thus, the prepared spinel $MnCo_2O_4$ is considered to be a well-crystallized structure with standard $MnCo_2O_4$ on nanoscale.

The specific surface areas and pore-size distribution are also important parameters closely related to the specific capacitance of electrode materials. Surface area and pore-size distribution analysis of $MnCo_2O_4$ were conducted using N_2 adsorption and desorption experiments. As seen from Fig. 3, the profile of the hysteresis loop indicates an adsorption-desorption characteristic of porous materials. The as-prepared $MnCo_2O_4$ has acceptable surface area of 89.67 $m^2\,g^{-1}$, which can keep the effective contact areas of active materials and electrolyte. It is well known that an increase in the electrode-electrolyte interfacial area can generate more active sites, which are beneficial for OH^- insertion and extraction, and thus increases the power performance at high current densities. Besides, the parameters of pore size and pore volume are also important factors for influencing power performance. The pore size distribution of as-prepared $MnCo_2O_4$ shows a wide peak centered at about 7 nm, which is falling in the optimal size for electron conduction and electrolyte transportation [26–29]. These features
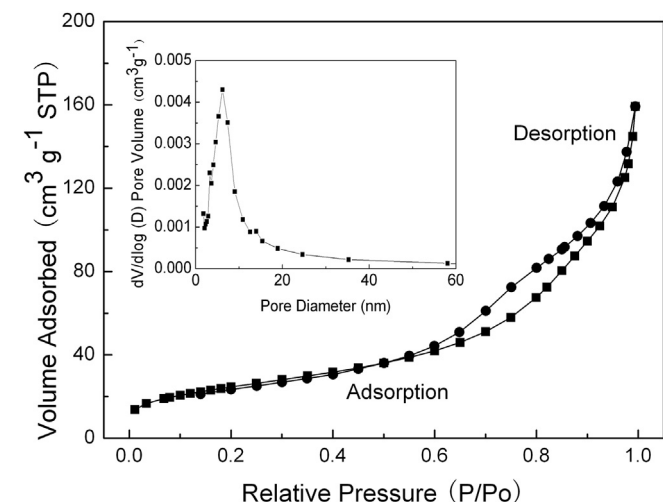
Fig. 3. The N$_2$ adsorption-desorption isotherm of MnCo$_2$O$_4$.

are of huge benefits for the transport and diffusion of electrolyte ions during the charge-discharge process.

3.2. Electrochemical measurements

CV measurements and galvanostatic charge-discharge test have been performed to evaluate the electrochemical properties and quantify the specific capacitance of as-prepared MnCo$_2$O$_4$ electrode. MnCo$_2$O$_4$ is regarded as a mixed valence oxide that adopts a spinel structure. Fig. 4a presents the CV behavior of MnCo$_2$O$_4$ at various scan rates. Three pairs of redox current peaks correspond to the reversible reactions, which indicates that the pseudo capacitance possibly comes from the Faradic redox reaction of Co^{2+}/Co^{3+}/Co^{4+} and Mn^{2+}/Mn^{3+}/Mn^{4+} [23,30–32]. Moreover, the capacitance characteristic is very distinguished from that of EDLCs which are rectangular CV curve. With the increase of scan rates, the shape of the CV curves changed, anodic peak potential and cathodic peak potential shifted in the more anodic and more cathodic direction, and the capacitance, inevitably, decreased, which is in agreement with the result of galvanostatic charge-discharge test.

The relationship between specific capacitance and current density is investigated. Fig. 4b displays the charge-discharge curves of MnCo$_2$O$_4$ within the potential range from 0 to 0.4 V. The specific capacitance of the curves can be calculated according to the following equation:

$$C_m = \frac{C}{m} = \frac{I \times \Delta t}{\Delta V \times m}$$

where C_m (F g^{-1}) is the specific capacitance, I (A) is discharge current, Δt (s) is the discharging time, ΔV (V) represents the potential drop during discharge process, and m (g) is the mass of the active material within the electrode. The as-prepared spinel MnCo$_2$O$_4$ exhibits excellent capacitive behavior at different current densities. The specific capacitance values calculated from discharge curves in Fig. 4b are 405, 384, 344, 309, 275, and 250 F g^{-1} at current densities of 5, 10, 20, 30, 40, and 50 mA cm^{-2}, respectively. Apparently, the specific capacitance is much higher than those of previously reported Mn-Co oxides. But at high current densities, as seen, the voltage drop is produced and finally the fading of specific capacitance appears. The large voltage drop may be explained by referring to OH$^-$ ions diffusion processes during the charging-discharging for the electrode [2]. As discharge current density increases, massive OH$^-$ ions are required to intercalate swiftly at the interface of electrode/electrolyte. However, relatively low concentration of OH$^-$ ions could not meet this demand. The slope variation of discharge
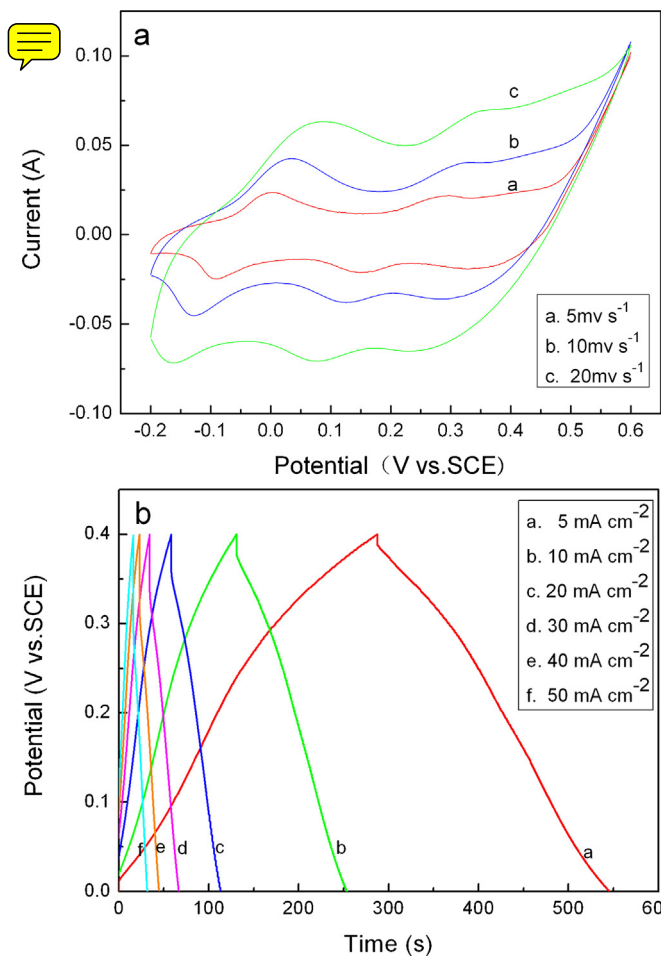
Fig. 4. (a) The CV curves of MnCo$_2$O$_4$; (b) The galvanostatic charge-discharge test curves of MnCo$_2$O$_4$.

curves has not been observed during the charge-discharge process compared with other metal oxides [33], exhibiting excellent capacitive behavior and promise for application in supercapacitors. The specific capacitance values of products calcined at 200, 250, 300, and 350 °C have been compared in Fig. 5. First of all specific capacitance gradually decreased at higher current density due to the
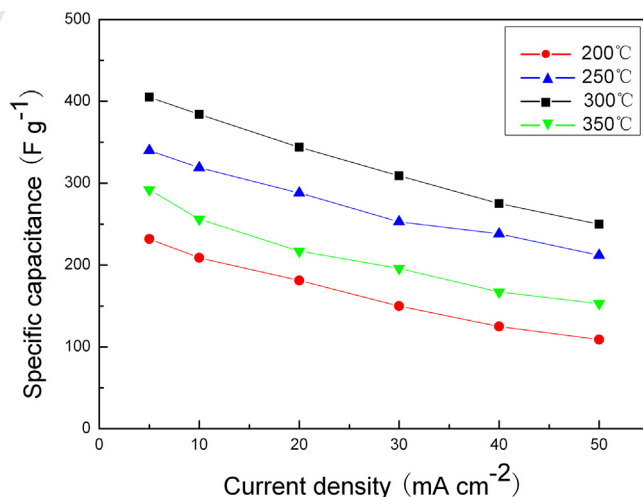
Fig. 5. The specific capacitance of products calcined at 200, 250, 300 and 350 °C, respectively.
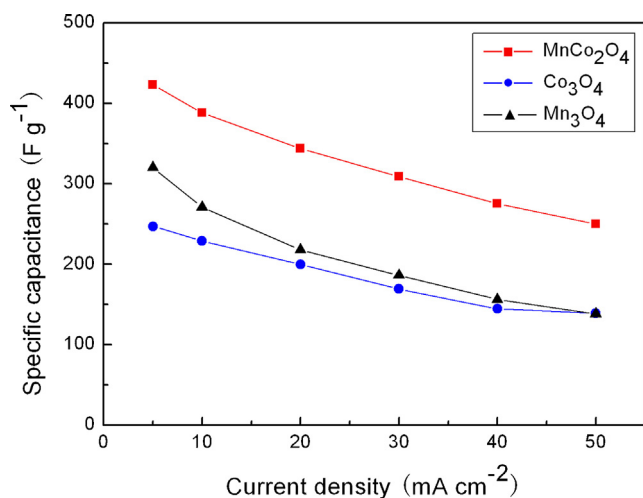
Fig. 6. The specific capacitance of $MnCo_2O_4$, Mn_3O_4 and Co_3O_4.
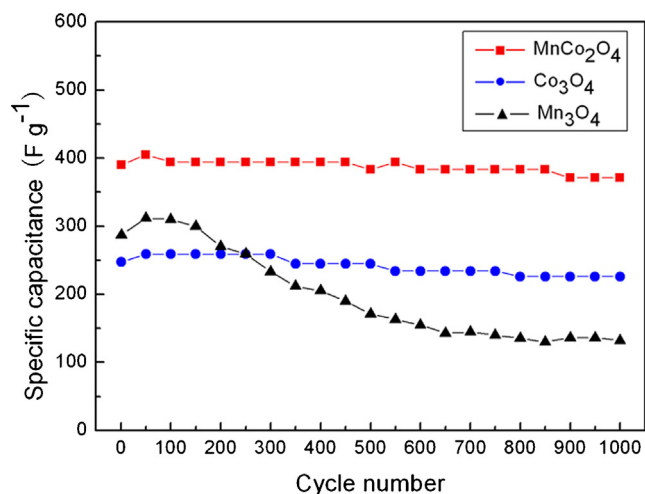

Fig. 8. The electrochemical stability test curves of $MnCo_2O_4$, Mn_3O_4 and Co_3O_4.

incremental voltage drop and insufficient active material involved in redox reaction at a higher current density. In addition, the specific capacitance increases as the thermal treatment temperature increases. The removal of water molecules, together with purity of products, was the key factor. However, the decrease of specific capacitance at 350 °C is possibly due to the growth of crystal grain. The specific capacitance values of $MnCo_2O_4$, Mn_3O_4 and Co_3O_4 are also compared in Fig. 6. It depicts that the specific capacitance of $MnCo_2O_4$ electrode is obviously much higher than those of the single component electrodes, i.e., the Mn_3O_4 and Co_3O_4 electrode. In practice, the ability to discharge at high rates is also crucial in capacitors. The discharge capacitance of $MnCo_2O_4$, Mn_3O_4 and Co_3O_4 at 40 mA cm^{-2} keeps 67.9%, 48.0% and 58.4% of those discharged at 5 mA cm^{-2}, respectively. Obviously, $MnCo_2O_4$ electrode exhibits good rate capability which makes it attractive particularly for a practical application.

In order to get more information about the ability of as-prepared $MnCo_2O_4$, EIS experiments were carried out in 2 M KOH aqueous solution at 0.3 V (vs. SCE). The frequency explored was from 10^{-2} to 10^5 Hz. Fig. 7 shows the EIS in the form of plots of $MnCo_2O_4$, Mn_3O_4 and Co_3O_4 where Z' and Z'' are the real and imaginary parts of the impedance. All the impedance plots were similar, being composed of one semicircle component at high frequency followed by a line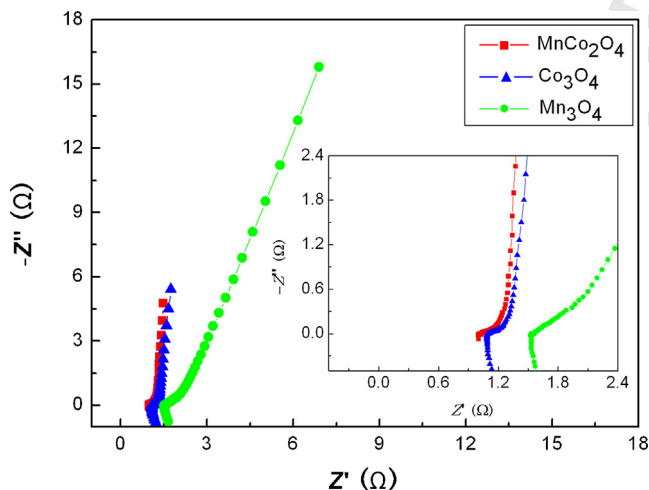ar component at the low frequency. From the data shown in Fig. 7, the electrode resistances of $MnCo_2O_4$, Mn_3O_4 and Co_3O_4 electrode, obtained from the intercept of the plots on real axis, are about 1, 1.5, and 1.2 Ω cm^{-2}. The semicircle corresponds to the pseudo charge transfer resistance (R_{ct}) [34]. The values of charge transfer resistance of $MnCo_2O_4$, Co_3O_4, and Mn_3O_4 are about 0.15, 0.2, and 0.4 Ω. Besides, at lower frequency, the straight line represents the diffusive resistance (Warburg impedance) of the electrolyte ions in host material. Compared with Mn_3O_4 and Co_3O_4, $MnCo_2O_4$ shows the lowest Warburg impedance [35].

Long cycle life at high current density is a prerequisite requirement for electrode materials. Hence, the cycling stability of $MnCo_2O_4$, Mn_2O_3 and Co_3O_4 was performed by charge-discharge test at a current density of 10 mA cm^{-2}. As shown in Fig. 8, after 1,000 cycles of charge-discharge, the specific capacitance of Mn_3O_4 and Co_3O_4 degraded by 51.5% and 8.7%, respectively. The great attenuation of Mn_3O_4 can be correlated with the dissolving in KOH electrolyte. By contrast, the spinel $MnCo_2O_4$ electrode, however, the specific capacitance suffered only a loss of 4.9% without any dissolution, suggesting its good stability in alkaline electrolyte. On the one hand, a tiny fraction of electroactive material fell off the nickel foam since the working electrode was immersed in electrolyte for a long time. On the other hand, the capacitance loss was possibly due to the irreversible Faraday reactions or the microstructure in the process of OH$^-$ insertion (extraction) during oxidation (reduction) [36]. Clearly, such high cycling stability of $MnCo_2O_4$ is much better than those of Mn_3O_4, Co_3O_4 and reported Mn-Co oxides. Overall, spinel $MnCo_2O_4$ displayed superior cycling stability in long-term cycles.

On the basis of above experimental evidence, the serial results effectively prove that spinel $MnCo_2O_4$ has desirable specific capacitance, high power performance, and excellent cycle performance. The well-connected porous structure is crucial to improve the electrochemical properties. On the one hand, the macropores can serve as ion-buffering reservoirs to minimizing the diffusion distance to the interior surfaces, which may accelerate the kinetic process of the ion diffusion in the electrode. On the other hand, the mesopores possess the ability to hold the electrolyte and facilitate the transport and diffusion of electrolyte ions during the charge-discharge process. Furthermore, the outstanding stability in alkaline electrolyte is a key factor to the high capacitance and high cycling life. It highlights once again that the microstructure of electrode materials is important for electrochemical performance in long-term cycles.

Fig. 7. The EIS curves of $MnCo_2O_4$, Mn_3O_4 and Co_3O_4.

4. Conclusion

In summary, the spinel $MnCo_2O_4$ electrode material was fabricated with a low-cost sol–gel method and the capacitive behavior was successfully investigated in alkaline electrolyte. The spinel $MnCo_2O_4$ displayed high specific capacitance (405 F g^{-1} at 5 mA cm^{-2}), remarkable rate capability (67.9% capacity retention at 40 mA cm^{-2}), and excellent cycle stability (only 4.9% loss after 1,000 cycles). It should not be ignored that the porous structure and fairly stable spinel structure played very important roles in improving specific capacitance, power performance, and cycle stability. Meanwhile, the present work displays the design of next generation of low-cost and ultra-high-performance binary metal oxide electrode materials prepared by facile method. Therefore, the as-prepared spinel $MnCo_2O_4$ is considered as a promising electrode material for supercapacitor applications.

References

[1] B.E. Conway, Electrochemical Supercapacitors: Scientific Fundamentals and Technological Applications, Kluwer Academic/Plenum, New York, 1999.
[2] R. Kötz, M. Carlen, Electrochim. Acta 45 (2000) 2483.
[3] T.Y. Wei, C.H. Chen, H.C. Chien, S.Y. Lu, C.C. Hu, Adv. Mater. 22 (2010) 347.
[4] Y.Y. Gao, S.L. Chen, D.X. Cao, G.L. Wang, J.L. Yin, J. Power Sources 195 (2010) 1757.
[5] Z. Fan, J.H. Chen, K.Z. Cui, F. Sun, Y. Xu, Y.F. Kuang, Electrochim. Acta 52 (2007) 2959.
[6] T.Y. Wei, C.H. Chen, K.H. Chang, S.Y. Lu, C.C. Hu, Chem. Mater. 21 (2009) 3228.
[7] L. Yang, S. Cheng, Y. Ding, X.B. Zhu, Z.L. Wang, M.L. Liu, Nano Lett. 12 (2012) 321.
[8] M.C. Liu, L.B. Kong, C. Lu, X.M. Li, Y.C. Luo, L.K., X.H. Li, F.C. Walsh, J. Electrochem. Soc. 159 (2012) A1262.
[9] Y.C. Hsieh, K.T. Lee, Y.P. Lin, N.L. Wu, S.W. Donne, J. Power Sources 177 (2008) 660.
[10] Q. Li, K. Li, J. Gu, H. Fan, J. Phys. Chem. Solids 69 (2008) 1733.
[11] T. Brousse, M. Toupin, R. Dugas, L. Athouel, O. Crosnier, D. Belanger, J. Electrochem. Soc. 153 (2006) A2171.
[12] B. Babakhani, D.G. Ivey, J. Power Sources 195 (2010) 2110.
[13] M. Toupin, T. Brousse, D. Bélanger, Chem. Mater. 14 (2002) 3946.
[14] H.Y. Lee, J.B. Goodenough, Electrochem. Solid State Lett. 4 (2001) A19.
[15] H. Li, G. Zhu, Z.H. Liu, Z. Yang, Z. Wang, Carbon 48 (2010) 4391.
[16] M.R. Tarasevich, B.N. Efremov, in: S. Trasatti (Ed.), Electrodes of Conductive Metallic Oxides Part A, Elsevier, USA, 1982.
[17] W.F. Wei, W.X. Chen, D.G. Ivey, Chem. Mater. 19 (2007) 2816.
[18] W.F. Wei, W.X. Chen, D.G. Ivey, J. Phys. Chem. C 111 (2007) 10398.
[19] W.F. Wei, W.X. Chen, D.G. Ivey, Chem. Mater. 20 (2008) 1941.
[20] K.R. Prasad, N. Miura, Electrochem. Commun. 6 (2004) 1004.
[21] J.K. Chang, M.T. Lee, C.H. Huang, W.T. Tsai, Mater. Chem. Phys. 108 (2008) 126.
[22] D.F. Yang, J. Power Sources 198 (2012) 416.
[23] P.Y. Chuang, C.C. Hu, Mater. Chem. Phys. 92 (2005) 138.
[24] B. Babakhani, D.G. Ivey, Electrochem. Acta 56 (2011) 4757.
[25] D.W. Wang, F. Li, M. Liu, G.Q. Lu, H.M. Cheng, Angew. Chem., Int. Ed. 47 (2008) 373.
[26] H. Zhou, D. Li, M. Hibino, I. Honma, Angew. Chem. Int. Ed. 44 (2005) 797.
[27] K.H. Chang, C.C. Hu, Appl. Phys. Lett. 88 (2006) 193102.
[28] C.C. Hu, K.H. Chang, M.C. Lin, Y.T. Wu, Nano Lett. 6 (2006) 2690.
[29] D.N. Futaba, K. Hata, T. Yamada, T. Hiraoka, Y. Hayamizu, Y. Kakudate, O. Tanaike, H. Hatori, M. Yumura, S. Iijima, Nat. Mater. 5 (2006) 987.
[30] P. Cosse, J. Inorg, Nucl. Chem. 8 (1958) 483.
[31] W.L. Roth, J. Phys. Chem. Solids 25 (1964) 1.
[32] H.W. Wang, Z.A. Hu, Y.Q. Chang, Y.L. Chen, H.Y. Wu, Z.Y. Zhang, Y.Y. Yang, J. Mater. Chem. 21 (2011) 10504.
[33] X.F. Wang, D.B. Ruan, Z. You, Trans. Nonferrous Met. Soc. China 16 (2006) 1129.
[34] M.S. Wu, H.H. Hsieh, Electrochim. Acta 53 (2008) 3427.
[35] L.P. Zheng, X.Y. Wang, H.F. An, X.Y. Wang, L.H. Yi, L. Bai, J Solid State Electrochem. 15 (2011) 680.
[36] C.Z. Yuan, X.G. Zhang, L.H. Su, B. Gao, L.F. Shen, J. Mater. Chem. 19 (2009) 5772.